

Under consideration for publication in *ASME Journal of Biomechanical Engineering*

The role of finite displacements in vocal fold modeling

Siyuan Chang, Fang-Bao Tian, and Haoxiang Luo

*Department of Mechanical Engineering, Vanderbilt University
2301 Vanderbilt Pl., Nashville, TN 37235*

James F. Doyle

*School of Aeronautics and Astronautics, Purdue University
West Lafayette, IN 47907-2045, USA*

Bernard Rousseau

*Departments of Otolaryngology and Hearing and Speech Sciences, Vanderbilt University
1215 21st Ave. South, Nashville, TN 37232*

Abstract

Human vocal folds experience flow-induced vibrations during phonation. In previous computational models, the vocal fold dynamics has been treated with linear elasticity theory in which both the strain and the displacement of the tissue are assumed to be infinitesimal (referred to as model I). The effect of the nonlinear strain, or the geometric nonlinearity, caused by the finite displacement is yet not clear. In this work, a two-dimensional model is used to study the effect of the geometric nonlinearity (referred to as model II) on the vocal fold and the airflow. The result shows that even though the deformation is under 1 mm, i.e., less than 10% of the size of the vocal fold, the geometric nonlinear effect is still significant. Specifically, model I underpredicts the gap width, the flow rate, and the impact stress on the medial surfaces as compared to model II. The study further shows that the differences are caused by the contact mechanics and more importantly, the fluid-structure interaction that magnifies the error from the small-displacement assumption. The results suggest that using the large-displacement formulation in a computational model would be more appropriate for accurate simulations of the vocal fold dynamics.

PACS numbers:

I. INTRODUCTION

Computational modeling of the vocal fold vibration is an important tool for studying the vocal fold dynamics and the physical process of voice production. In such a tool, a vocal fold model is typically coupled with an airflow model to simulate the fluid-structure interaction (FSI) during phonation. Recently, continuum mechanics based computer models have gained popularity compared to the earlier simple but nevertheless insightful lumped-mass models, e.g., two-mass models with connective springs^{1,2}. In the continuum models, the vocal fold tissue is treated as a continuously deformable medium using classical solid mechanics theory, which allows the deformations of the vocal fold to be captured in more detail. In a recent work, Alipour *et al.*³ have given a broad review of computational phonation in which they discussed extensively existing modeling techniques, primary research findings, and also the validation efforts.

Among many previous studies that have developed continuum models of the vocal fold, small deformations are often assumed for the vocal fold⁴⁻⁶. The rationale for this assumption is that during normal phonation, the displacement of the vocal fold is on order of 1 mm, which is much smaller compared to the characteristic length of the vocal fold, which is around 1 cm⁷. Thus, the strain is only approximately 10% for normal phonation. This assumption makes the model computation very efficient since the linear elasticity theory based on small deformations involves a linear strain measure and also a linear stress-strain relationship. In some recent work, nonlinear models have been adopted for the vocal fold. For example, Thomson and coworkers^{8,9} used a hyperelastic Ogden tissue model in their study of the geometric effect of the laryngeal configuration on the vocal fold dynamics. As a separate line of effort, Chan and his colleagues have worked on characterization of the nonlinear tissue properties and the effect of the nonlinear properties on the fundamental frequency of the vocal fold^{10,11}. Despite these efforts, a quantitative study on limitation of the linear assumption is still very limited, especially in the context of fluid-structure interaction. Further study may be necessary in order to develop accurate computational models that may find clinical applications.

In solid mechanics, several sources could introduce nonlinearity into the dynamics of a structure. Typical examples include the geometric nonlinearity, contact mechanics, and material nonlinearity¹². For a general solid experiencing arbitrary deformations, sometimes even when the strain is small, the displacement and accompanying rotation of some parts of the body can be large. A classical example is a cantilever beam bent under the transverse load, where the free end of the beam can go through large displacement and rotation even if the local strain anywhere in the beam is small. Such large displacement and rotation would lead to nonlinear formulation of the strain due to the significant change to the body configuration, a term referred to as geometric nonlinearity in solid mechanics¹². Therefore, in some cases the large-displacement formulation should be used for structural analysis even when the strain is only above 5%. As mentioned earlier, the vocal fold tissue may be around or somewhat exceeding this limit during normal phonation, and thus it would be worthwhile to investigate its geometric nonlinear effect.

Contact mechanics is involved in the vocal fold dynamics due to collision of the two folds at their medial surfaces. This effect has been included in many previous studies^{5,13,14} to investigate the impact stress on the vocal fold. Since contact mechanics is essentially a nonlinear process and it largely depends on the local geometry of the two surfaces¹⁵, a small error relative to the overall

dimension of the vocal fold could lead to significant change in the displacement of the local contact area and therefore, less accurate prediction of the impact stress. Furthermore, although the gap between the two vocal folds, i.e., the glottis, is small as compared to the size of the vocal folds, the airflow largely depends on the width and shape of the glottis, and the flow may in turn affect the pressure distribution on the vocal folds. However, it is not yet clear whether the error due to the small-displacement assumption would increase or not in the context of nonlinear fluid-structure interaction. A careful investigation of the issues described here would provide useful information on modeling errors and thus be helpful for future development of accurate vocal fold models.

We emphasize that the current discussion is still within the scope of the small-strain assumption. In real situations, large deformations (and thus large strains) of the vocal fold can happen as well, for example, due to substantial local deformation, lengthening of the vocal folds, or insertion of an implant. The large strain could lead to a nonlinear stress-strain relationship, i.e., material nonlinearity as referred to in solid mechanics, and it is beyond the scope of this work.

In this work, we will use a two-dimensional (2D) larynx model to study the effect of finite displacements on the characteristics of the vocal fold vibration and those of the glottal flow. The problem formulation and the theoretical background of geometric nonlinearity will be described in Section 2. Results and discussion will be provided in Section 3. Concluding remarks will be given in Section 4.

II. MODEL DESCRIPTION AND THE NUMERICAL APPROACH

A. Model setup

The two-dimensional vocal fold model is shown in Fig. 1, where the setup is similar to the one in Luo *et al.*¹⁶. A pair of vocal folds of identical properties are placed in a straight rectangular channel representing the passageway of the airflow. The channel length and height are $L = 12$ cm and $H = 2$ cm, respectively. The channel walls are rigid, but the vocal folds are elastic and can go through plane-strain deformations (i.e., deformation in the xy -plane only). Although the vocal fold tissue is known to be anisotropic and inhomogeneous¹⁷, here we simplify the problem by considering an isotropic and homogeneous tissue model. The tissue properties include the density $\rho_s = 1$ g/cm³, Young's modulus $E = 40$ kPa, and Poisson's ratio $\nu_s = 0.3$. These properties are within the ballpark of previous computational models^{4,13,16}.

The airflow is driven by a constant subglottal pressure, P_{sub} , at the inlet on the left end of the channel, and it varies from 0.5 to 0.8 kPa, and the outlet pressure, P_{out} , is set to be zero. The air is assumed to be Newtonian and incompressible, and its density and viscosity are respectively $\rho_f = 0.001$ g/cm³ and $\mu = 2 \times 10^{-4}$ Pa·s. The governing equations for the flow are the unsteady incompressible Navier–Stokes equations,

$$\frac{\partial v_i}{\partial t} + \frac{\partial v_i v_j}{\partial x_j} = -\frac{1}{\rho_f} \frac{\partial p}{\partial x_i} + \nu \frac{\partial^2 v_i}{\partial x_j \partial x_j}, \quad \frac{\partial v_i}{\partial x_i} = 0, \quad (1)$$

where v_i is the velocity component, p is the pressure, ρ_f is the density and ν is the kinematic viscosity. No-slip and no-penetration boundary conditions are imposed at the channel walls and also at the vocal fold surfaces. At the inlet and outlet, the normal shear stress is set to zero.

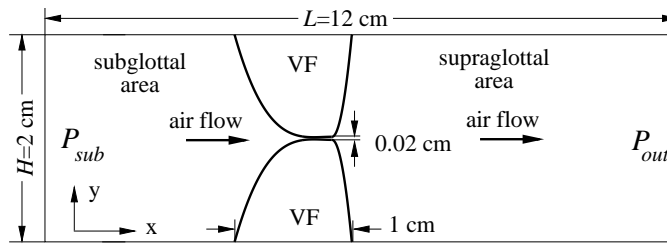


FIG. 1. A 2D model for studying the role of geometric nonlinearity in the vocal fold dynamics.

The vocal fold tissue is assumed to be linearly elastic, which is a suitable assumption when the strain is small. That is, the stress is linearly proportional to the strain. However, depending on whether the solid structure experiences significant displacement and significant rotational deformations (e.g., greater than 5%), the stress and strain measures are different. Two formulations are considered here. One of them is the commonly adopted small-displacement formulation, in which the stress σ_{ij} is linearly proportional to the strain ε_{ij} by the relationship¹².

$$\sigma_{xx} = (C_{11}\varepsilon_{xx} + C_{12}\varepsilon_{yy}), \quad \sigma_{yy} = (C_{12}\varepsilon_{xx} + C_{22}\varepsilon_{yy}), \quad \sigma_{xy} = 2G\varepsilon_{xy}, \quad (2)$$

where $G = E/(2 + 2\nu_s)$ is the shear modulus and C_{11} , C_{22} , C_{12} are the elasticity constants determined from E and ν_s ¹². The strain is also a linear function of the displacement, that is,

$$\varepsilon_{ij} = \frac{1}{2} \left(\frac{\partial u_i}{\partial x_j} + \frac{\partial u_j}{\partial x_i} \right), \quad (3)$$

where u_i is the displacement vector.

The other formulation assumes that the displacement and rotation are no longer small, and the strain measure becomes a nonlinear function of the displacement, which is termed geometric nonlinearity¹². Using the Lagrangian formulation, the strain can be written as

$$\varepsilon_{ij} = \frac{1}{2} \left(\frac{\partial u_i}{\partial X_j} + \frac{\partial u_j}{\partial X_i} + \frac{\partial u_k}{\partial X_i} \frac{\partial u_k}{\partial X_j} \right), \quad (4)$$

where X_i refers to a material point in the reference configuration (or the undeformed state). Note that compared with Eq. (3), Eq. (4) has higher-order terms from products of the linear deformation components. Such a formulation incorporates the nonlinear effect caused by rotation of entire or part of the body, e.g., the rigid-body-type rotation near the free tip of a cantilever beam when the displacement is large. In the case of vocal fold deformation, such rotational effect could happen to the vocal fold, if its cross section is viewed as a cantilever beam with the medial surface as the free end and the subglottal pressure as the load. Eq. (4) also takes into account of the finite deformation, if any, at the contact area during vocal fold impact. In the present work, we consider a simple material behavior, where the stress-strain formulation is the same as Eq. (2) except that the notation of the second piola-Kirchhoff stress¹², S_{ij} , would be used in place of σ_{ij} .

Henceforth we will refer to the first formulation as model I and the second as model II. Note that the present coupled flow-vocal-fold system is overall a nonlinear system no matter which constitutive

law is being used. Furthermore, the contact mechanics as discussed earlier adds another source of nonlinearity to the vocal fold dynamics in both models.

B. Numerical method

The numerical simulation is performed using the fluid-structure interaction package ADINA 8.8 (ADINA R&D Inc., Watertown, MA). This finite-element package has been previously used for vocal fold modeling^{8,9,18}. A triangular mesh of 12,850 nodes and 24,576 elements is used to discretize the flow domain shown in Fig. 1. Finer resolution is employed within the glottis and around the vocal fold surfaces. A triangular mesh of 385 nodes and 288 elements is used to discretize each vocal fold. For the transient analysis, a composite second-order method is adopted for the flow, while the Bathe integration method is chosen for the solid. The iterative solution option is chosen for the fluid-structure coupling. Descriptions of these choices can be found in the ADINA documentation. The time step is $\Delta t = 0.02$ millisecond (ms), which leads to about 250 steps for a vibration cycle of approximately 5 ms. The mass-damping coefficient and the stiffness-damping coefficients are chosen to be 0.015 and 0.0002, respectively, for the vocal folds. A minimum gap of 0.2 mm is assumed for the glottal gap. The two vocal folds are assumed to be in contact when they approach this specified limit. For the contact dynamics, the built-in penalty function is applied, which prevents the vocal folds from penetrating each other.

A grid convergence test is done for model II with $P_{\text{sub}} = 0.7$ kPa. In the test, the number of mesh elements are doubled and the simulation result is compared with that from the baseline simulation. The comparison shows that the differences of the two simulations in the glottal gap width, the oscillation frequency of the vocal folds, and the impact stress (definitions of these quantities will be given later) are only 2.64%, 0.1%, and 5.69%, respectively. Therefore, the original mesh is deemed acceptable for this work. Note that as the vocal folds move, the mesh will deform correspondingly, which is done automatically in ADINA. However, manual mesh regeneration and simulation restart are necessary in some cases, e.g., $P_{\text{sub}} = 0.8$ kPa, since the mesh distortion becomes severe. To make sure that the simulations are acceptable, a similar grid convergence test was done for these cases. The result shows that after mesh refinement, the change in the glottal gap width is less than 9% (i.e., much smaller as compared with the difference we will report between model I and model II) and the vibration behavior of the vocal fold does not vary significantly.

III. RESULTS AND DISCUSSIONS

In the current study we set the subglottal pressure P_{sub} to be 0.5, 0.6, 0.7, and 0.8 kPa. Further increase of P_{sub} would cause the mesh quality to deteriorate quickly and would require extensive manual mesh adjustment. For each value of P_{sub} , we run model I and model II separately; then we collect the statistics after onset of the vocal fold vibration is established. The simulations were typically run for 100 to 200 vibration cycles, and it takes 60 to 100 cycles to reach steady vibration. It was determined that steady vibration has been achieved when the averaged gap width over 20 cycles does not change significantly. The statistics are collected over 20 cycles during steady vibration. We will discuss the vibration characteristics, the impact stress at the medial surfaces,

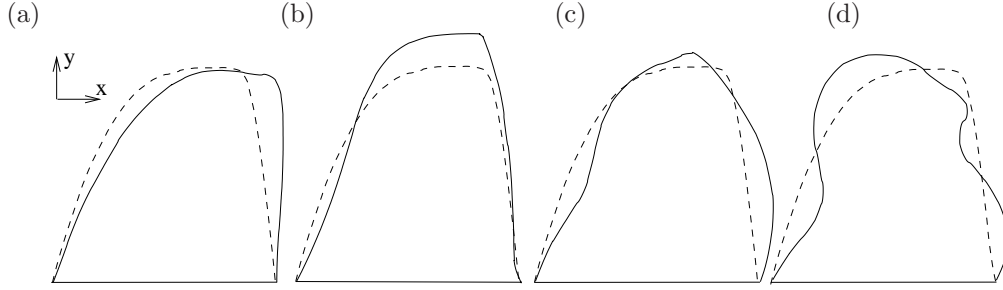


FIG. 2. The lowest four eigenmodes of the current vocal fold model. (a) The 1st mode at $f_1 = 86.9$ Hz, (b) the 2nd mode at $f_2 = 192.2$ Hz, (c) the 3rd mode at $f_3 = 217.5$ Hz, and (d) the 4th mode at $f_4 = 372.9$ Hz. The dashed line is for the rest shape, and the solid line is for deformed shape.

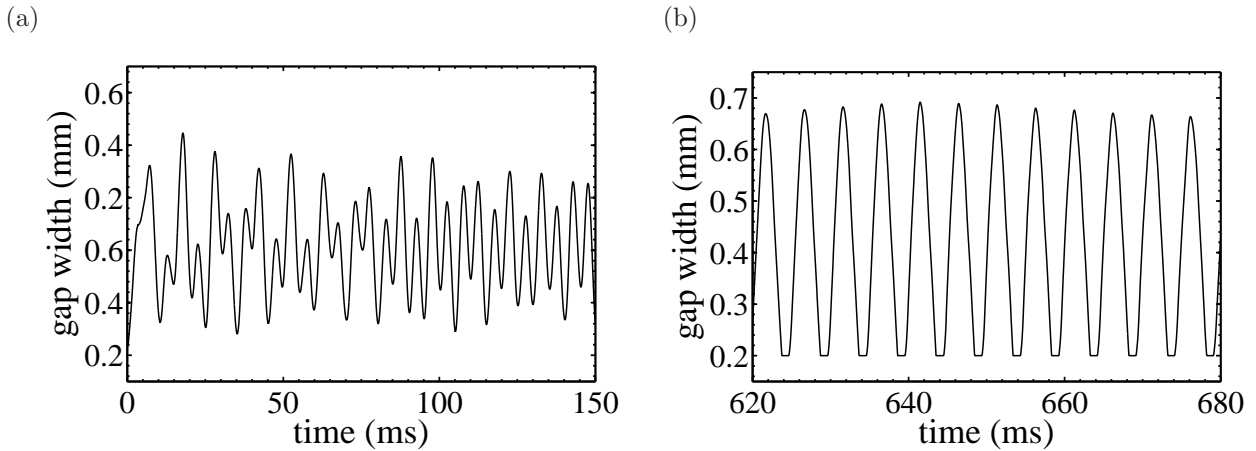


FIG. 3. The time history of the glottal gap width for model II with $P_{\text{sub}} = 0.6$ kPa. (a) Initial transition period; (b) the established vibration.

and the flow behavior for each model.

A. Frequency and mode of vocal fold vibration

An eigenmode analysis is first performed for the current vocal fold model. The analysis will help us discuss the vibration pattern of the vocal folds induced by the flow. Figure 2 shows the lowest four eigen modes along with the corresponding eigenfrequencies. These modes are qualitatively similar to those of a three-layer, two-dimensional vocal fold model used by Luo *et al.*¹⁶. In addition, the spectrum of the eigenfrequencies is also close to that in Luo *et al.*¹⁶. That is, the lowest frequency is near $f_1 = 100$ Hz; the second and the third frequencies, f_2 and f_3 are both roughly twice of f_1 ; and the fourth frequency, f_4 , is roughly four times of f_1 . Therefore, using the single-material model does not change the characteristics of the vocal folds qualitatively.

Figure 3 shows a typical time history of the glottal gap width, defined as the smallest gap between the two vocal folds projected along the y -direction, for both the transient period (Fig. 3(a)) and later established vibration (Fig. 3(b)). In this figure, $P_{\text{sub}} = 0.6$ kPa and model II is used. It can be seen that the vocal folds first oscillate at a lower frequency and then a higher-frequency mode appears and finally takes over. A further inspection shows that these two frequencies are respectively close to the first and the second eigenfrequencies. Therefore, the current vocal folds go through a modal transition during the onset of vibration. This result is consistent to the report in Luo *et al.*⁵.

The dominant vibration frequency of the vocal folds during steady vibration are tabulated in Table I for both model I and model II. The frequency is calculated based on the y -displacement of a point on the medial surface (shown in Fig. 4(a)). It can be seen that except for the case of model I at $P_{\text{sub}} = 0.8$ kPa, the frequency in all other cases is near the second eigenfrequency $f_2 = 192.2$ Hz. Furthermore, the results from model I and model II are very close to each other. However, at $P_{\text{sub}} = 0.8$ kPa the two models have significantly different results. The frequency from model II remains near f_2 , but the frequency from model I is higher and is actually closer to the third eigenfrequency $f_3 = 217.5$ Hz.

We further examine the vibration patterns shown in Fig. 4 for the cases of $P_{\text{sub}} = 0.6$ kPa to 0.8 kPa. It can be seen that at $P_{\text{sub}} = 0.6$ and 0.7 kPa, both model I and model II produce a pattern that is similar to the second mode, albeit the amplitude of vibration is greater in model II. The case with $P_{\text{sub}} = 0.5$ kPa, not shown here, is similar to that of $P_{\text{sub}} = 0.6$ kPa except that the amplitude of vibration is smaller. At $P_{\text{sub}} = 0.8$ kPa, the vibration from model II still has a second-mode pattern, and the amplitude becomes further increased as compared to that for $P_{\text{sub}} = 0.7$ kPa. However, for model I the vibration pattern at this higher subglottal pressure resembles the third eigenmode shown in Fig. 2(c), and this result is consistent with the oscillation frequency of this case. In this particular pattern, The inlet and the exit of the glottal gap open/close alternately; and the maximum width of the glottis is thus always limited. This gap width effect will be further discussed later. To explain a plausible cause for the behavior of model I at $P_{\text{sub}} = 0.8$ kPa, we note that the second eigenmode and the third eigenmode of the present vocal fold model are close to each other in terms of the frequency (192.2 Hz and 217.5 Hz, respectively). Furthermore, the temporal/spatial variations of the pressure in the glottis could allow either oscillation pattern to actually take place. Therefore, the present coupled fluid-structure system may have two stable periodic orbits that are close to each other, and it could be possible that due to change of P_{sub} or system description (i.e., linear v.s. nonlinear strain), the system settles down to a different orbit (vibration state).

Figure 5 shows the power spectrum density (PSD) analysis of the steady oscillation of the y -displacement of a point on the medial surface (shown in Fig. 4(a)) for $P_{\text{sub}} = 0.7$ kPa and 0.8 kPa. It can be seen that in all cases except model I at $P_{\text{sub}} = 0.8$ kPa, the power spectrum is dominated by the single frequency that is close to the second mode frequency f_2 . For model I at $P_{\text{sub}} = 0.8$ kPa, the third mode is dominant as discussed earlier, but the second mode is also significant. The PSD result in the cases of $P_{\text{sub}} = 0.5$ and 0.6 kPa is not shown here since their frequency component is similar to that in the case of $P_{\text{sub}} = 0.7$ kPa.

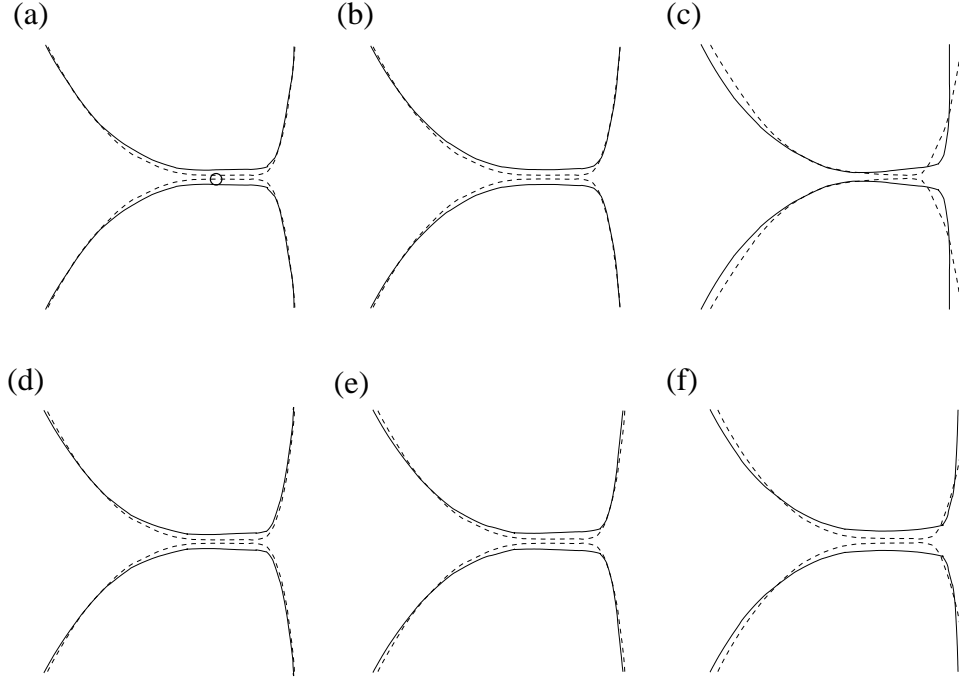


FIG. 4. The vibration pattern of the vocal folds simulated by model I (a,b,c) and model II (d,e,f). The subglottal pressure is (a,d) $P_{\text{sub}} = 0.6$ kPa, (b,e) $P_{\text{sub}} = 0.7$ kPa and (c,f) $P_{\text{sub}} = 0.8$ kPa. The solid line and dashed line represent the open and closed phases, respectively. The circle shown in (a) is the marker point that will be used in the PSD analysis.

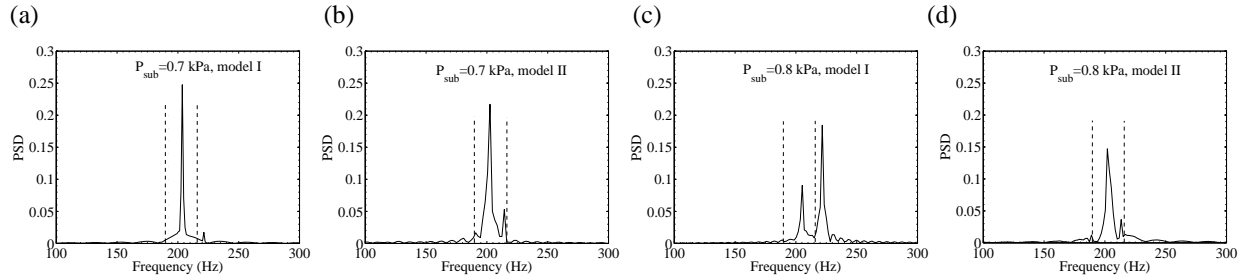


FIG. 5. The PSD analysis of the oscillation of a point at the medial surface for $P_{\text{sub}} = 0.7$ and 0.8 kPa. The two dashed lines indicate the eigenfrequencies f_2 and f_3 .

B. Gap width, waveform, and impact stress

Figure 6(a) shows the relationship between the maximum glottal gap width and subglottal pressure for both model I and model II. In general, the glottal gap width increases when the subglottal pressure is raised, which is consistent with previous studies¹⁷. An exception is in the case of model I with $P_{\text{sub}} = 0.8$ kPa. As discussed earlier, this case has a different vibration mode

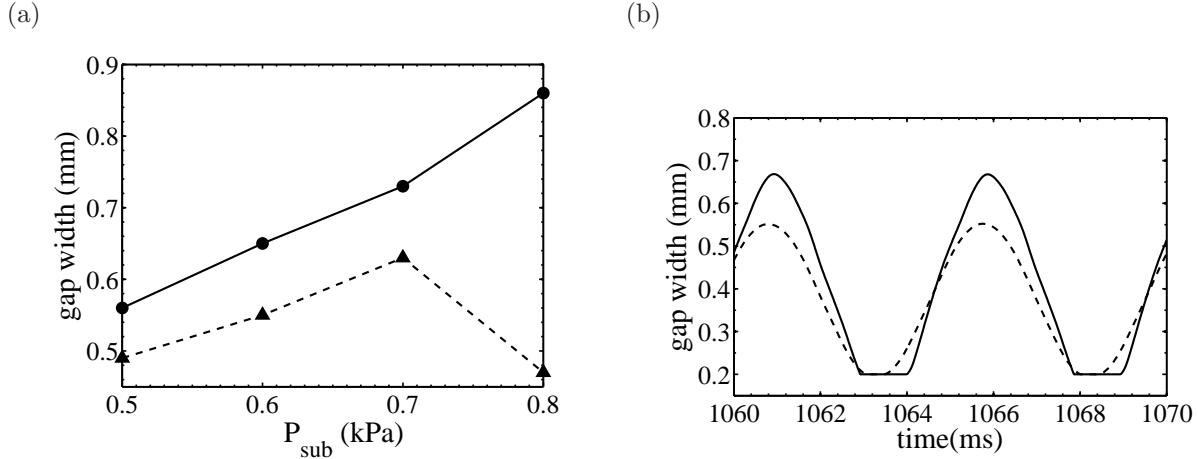


FIG. 6. (a) The gap width during the open phase versus P_{sub} . (b) The waveform of the gap width at $P_{\text{sub}} = 0.6$ kPa. In both (a) and (b), the dashed line is for model I and the solid line for model II.

that leads to a smaller gap width. The figure shows that model II consistently gives a greater magnitude of the gap width than model I. For P_{sub} between 0.5 and 0.7 kPa, the difference between the two models is less than 0.1 mm, but it still represents about 15% of increase for model II. At $P_{\text{sub}} = 0.8$ kPa, the difference between the two models is clearly large. Figure 6(b) shows the waveform of the gap width at $P_{\text{sub}} = 0.6$ kPa. We see that the waveforms have almost the same profile for the two models since the vocal folds are vibrating at the same mode at this pressure. However, the closed phase, or the contact time, of the vocal folds in model II is approximately 40% longer than that of model I.

The impact stress on the medial surface of the vocal folds during collision is an important quantity of interest, as it is likely the main contributing factor of phonotrauma¹⁹. Figure 7(a) shows the relationship between the impact stress and the subglottal pressure. The impact stress is calculated by averaging the stress during vocal fold collision at the contact area. At $P_{\text{sub}} = 0.5$ kPa, the vocal folds as predicted by model I did not reach the contact limit, and the impact stress is thus zero. As the subglottal pressure is raised from 0.5 kPa to 0.8 kPa, the magnitude of the impact stress is increased from 0.5 kPa to 1.5 kPa, which is generally in the data range of previous work¹⁴.

Comparing model I and model II, we see that model II always has greater impact stress than model I, and the difference is consistently around 0.4 kPa. As greater impact also leads to a larger contact area, we also plot the total contact force per unit span in each case. The result in Figure 7(b) shows that the contact force increases as P_{sub} is raised, as expected. In addition, the difference between model I and model II becomes more pronounced at higher values of the subglottal pressure. At $P_{\text{sub}} = 0.8$ kPa, this difference is about 1.7 N/m. A further inspection shows that the locations of the maximum impact at $P_{\text{sub}} = 0.8$ kPa are also different between the two models. This result can be seen from the shape of the closed glottis in Fig. 4. For model II, the greatest impact takes place in the middle of the medial surface (Fig. 4(f)), which is also the

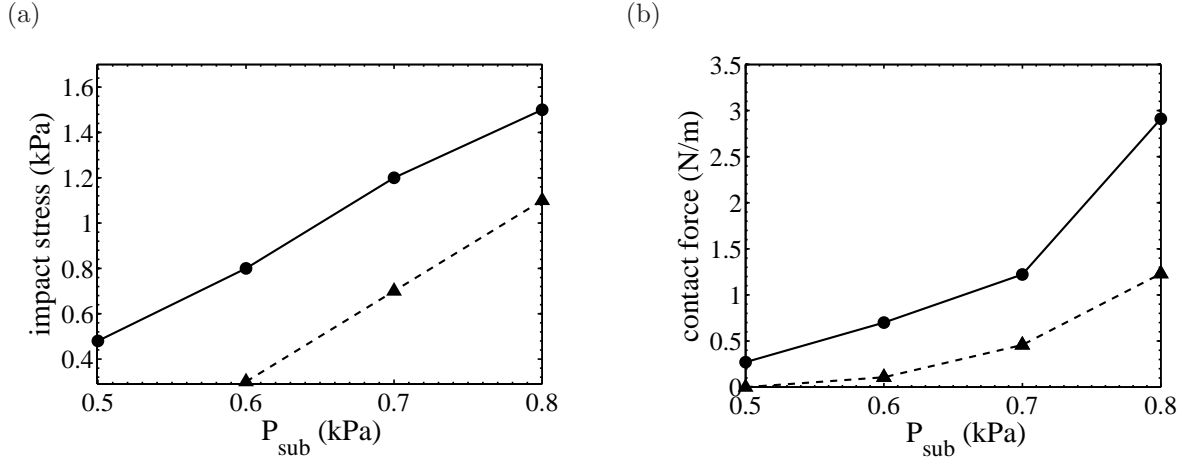


FIG. 7. The impact stress (a) and the total contact force (per unit length in span) (b) during vocal fold collision. The dashed line is for model I and the solid line for model II.

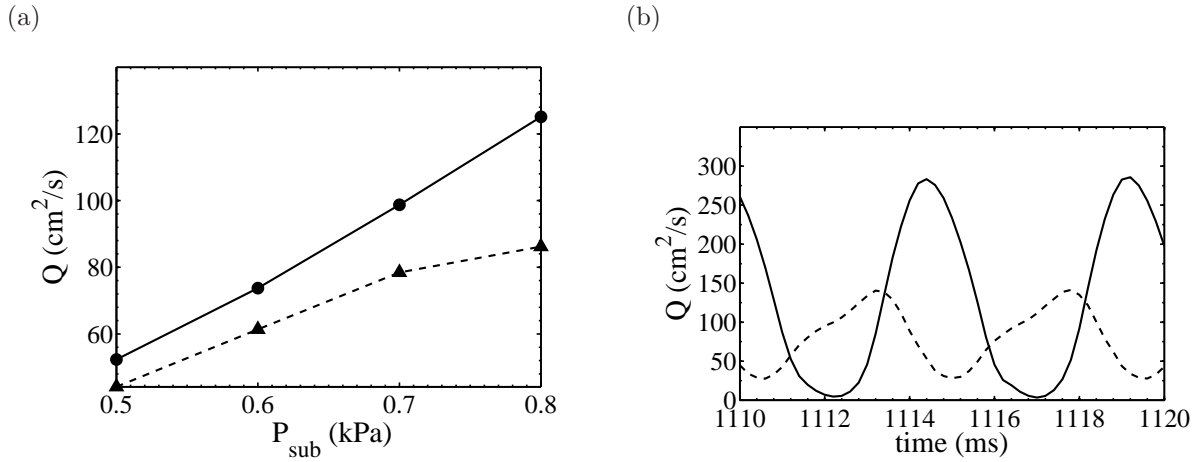


FIG. 8. (a) The time-averaged flow rate (per unit span); (b) the waveform of the flow rate at $P_{\text{sub}} = 0.8$ kPa. The dashed line is for model I and the solid line for model II.

case for the lower values of P_{sub} in Fig. 4. For model I, Fig. 4(c) shows that the greatest impact instead takes place near the glottal exit.

C. Flow characteristics

Figure 8(a) shows the flow rate, Q , averaged in time, from the two models. The flow rate increases nearly linearly with the subglottal pressure for model II. For model I, the flow rate is lower than that of model II for all levels of the subglottal pressure, and this result is consistent

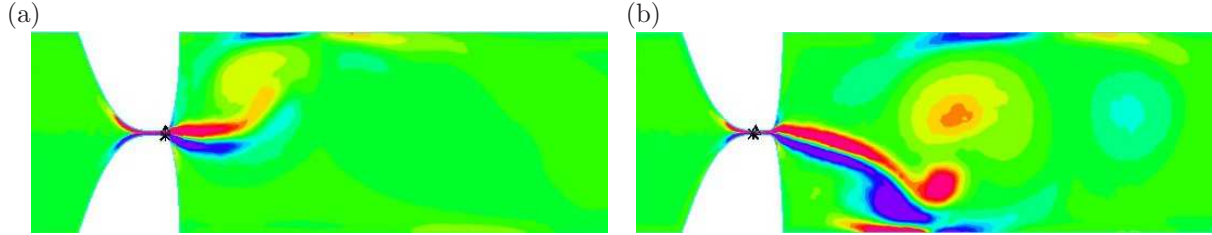


FIG. 9. Instantaneous vorticity contours during vocal fold opening for (a) model I and (b) model II at $P_{\text{sub}} = 0.8$ kPa.

with the result comparison on the glottal gap width as discussed earlier. At $P_{\text{sub}} = 0.8$ kPa, the flow rate given by model I becomes much lower than that of model II, and this result is due to the different vibration modes in the two models as discussed earlier. In this case, $Q = 124$ cm²/s for model II, and for model I the flow rate is only $Q = 83$ cm²/s. From the waveform plotted in Fig. 8, the flow rate in model I not only has a lower magnitude but also has a significantly different temporal profile than that in model II.

The vorticity plot indicates that when P_{sub} is increased, the flow fields from models I and II become significantly different from each other. Figure 9 shows the comparison of the instantaneous vorticity during the maximum opening phase between the two models at $P_{\text{sub}} = 0.8$ kPa. Compared to the cases with low P_{sub} , the jet Reynolds number, defined as $Re = 3Q/2\nu$, is higher at $P_{\text{sub}} = 0.8$ kPa, and thus the flow field is more complex. In addition, at higher P_{sub} , the jet becomes more asymmetric and its skewness varies from cycle to cycle. Discussed in detail in Luo *et al.*¹⁶, these phenomena are typical for the glottal airflow, and they are present in both models from the figure. However, we see that the jet is clearly stronger in model II than in model I, as in model II the jet has longer penetration length and produces stronger vortices downstream.

D. Further discussion

In the present study, the subglottal pressure is no greater than 0.8 kPa and is not particularly high as compared with the range of the normal phonation pressure¹⁷, and the deformation magnitude of the vocal folds is less than 1 mm, i.e., 10% of the size of the vocal folds. However, significant differences are produced by using model II in the predicted glottal gap width, impact stress, and flow characteristics. Note that in human phonation, the displacement up to 2 mm has been reported for the vocal folds¹⁹. To investigate the source that has caused such differences, two additional tests are introduced where the flow is assumed to be absent and the load on the vocal folds are manually specified. In the first test, a single vocal fold identical with those in the present FSI study is considered, and a uniform and static load p is applied on the subglottal and medial surfaces as shown in Fig. 10(a). In the second test, the load is sinusoidal with the amplitude p and the frequency at 200 Hz, and both vocal folds are present so that collision would occur. For both tests, we compare the displacement of the vocal folds calculated from model I with that from model II.

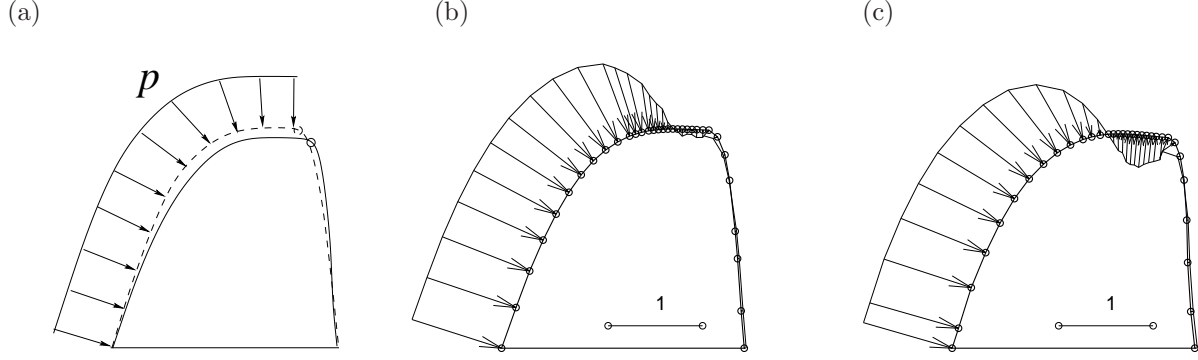


FIG. 10. (a) Illustration of the load tests of the current vocal fold model. The reference point marked by a circle is used to measure the displacement. (b,c) p/P_{sub} from the FSI simulation during vocal fold opening for (b) $P_{\text{sub}} = 0.6$ kPa and (c) $P_{\text{sub}} = 0.8$ kPa.

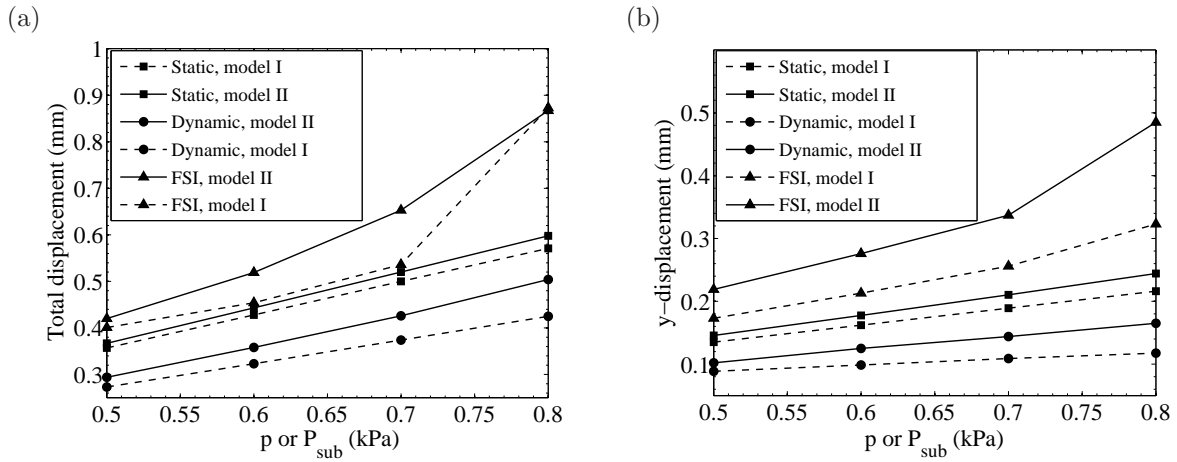


FIG. 11. Displacement of the reference point in the static load test, the dynamic load test, and the coupled FSI simulation. (a) The total displacement; (b) the y -displacement.

Figure 11 shows the result from the static test and the dynamic test. For comparison, we have also included the results from the coupled vocal-fold/flow simulation. The displacement of a point at the supraglottal exit as shown in Fig. 10 is used for such comparison. The magnitude of the load p is raised from 0.5 kPa to 0.8 kPa, to be consistent with the subglottal pressure used in the FSI simulation. Both the y -displacement and the total displacement (i.e., both x and y components included) are shown for the reason that will be explained soon.

Figure. 11(a) shows that in the static test, the total displacement from model I is near 0.6 mm at $p = 0.8$ kPa. Model II predicts only slightly greater deformation than model I at all load levels, and the difference is about 5% for $p = 0.8$ kPa. In the dynamic test, the relative difference between the two models becomes more significant than in the static test. As p is increased to 0.8

kPa, we see that the difference between the two models becomes more evident. This result can be explained since the contact of the two solid surfaces is a nonlinear function of the deformation and the difference between the two present structural models can be increased through the contact process.

When the airflow is introduced in the simulation, the total displacement of the vocal folds is in general greater than those in the no-flow tests, as shown in Fig. 11(a). In Fig. 10(b,c) we plot the pressure over the vocal fold surface normalized by P_{sub} for $P_{\text{sub}} = 0.6$ and 0.8 kPa. From these plots, we see that the pressure changes rapidly along the medial surface as expected. More importantly, the normalized pressure distribution in the case of $P_{\text{sub}} = 0.8$ kPa is significantly differently from that of $P_{\text{sub}} = 0.6$ kPa. This change of loading status thus helps to explain why the displacements shown in Fig. 11 are not linearly proportional to P_{sub} for the FSI cases. At $P_{\text{sub}} = 0.8$ kPa, the total displacement is near 0.9 mm, i.e., 9% of the size of the vocal folds, for both model I and model II. This total displacement is mostly in the x -direction due to the mean displacement of the vocal folds. The rotational effect and the coupling the x - and y - components of deformation due to this mean displacement have been incorporated in the geometric nonlinear formulation, as discussed in Section II.A. Since the y -component of the displacement is not necessarily linearly proportional to the x -component and the y -component is critical in determining the glottal opening, we show a comparison of this component in Fig. 11(b). In this figure, the comparisons of model I and model II in the static and the dynamic tests are similar to those shown in Fig. 11(a). That is, the difference between the two models is more pronounced in the dynamic test where contact is present. For the FSI simulation, the y -displacement from model I is 0.32 mm, which is significantly smaller as compared to 0.49 mm from model II and represents a larger difference than in the no-flow cases. Note in both no-flow and and FSI tests, the only difference between model I and model II is that geometric nonlinearity of the vocal folds is included in model II. From these test results, we see that the error due to ignoring geometric nonlinearity in modeling the vocal fold dynamics could be amplified through the interaction of the vocal folds with the flow and consequently lead to significant error in the prediction of the coupled system.

IV. CONCLUSION

We have numerically studied the flow-induced vocal fold vibration using a two-dimensional computational model under assumption of small strains. The vocal fold tissue is assumed to be linearly elastic but no restriction is required for its displacement and rotation so that the effect of geometric nonlinearity has been included in the model. By comparing this model with the previously commonly adopted small-displacement model (model I), we studied the effect of the finite displacement (model II) on the vocal fold dynamics and also on the glottal airflow.

The simulation result shows that model I produces consistently a smaller vibration amplitude for the subglottal pressure considered and consequently, the impact stress and the flow rate are significantly lower than those obtained from model II. In some cases, even the vibration mode of the vocal fold predicted by model I is different from that by model II, e.g., for the subglottal pressure at 0.8 kPa in the present study. Further investigation shows that the nonlinear effect is significant when the contact process and in particular, the flow-vocal-fold interaction, are involved, both of

which are sensitive to the displacement of the vocal folds.

In the case of phonation, the width and shape of the glottis are determined by the vocal fold displacement, and errors in predicting the vocal fold displacement may lead to significant change to the glottis and therefore to the vocal fold collision and the glottal airflow. The present study is limited to two dimensions and the isotropic/homogeneous tissue properties, and the quantitative results reported here may not be directly applicable to the vocal models in the previous studies or to the real vocal fold tissue. However, it suggests that for the sake of caution, including geometric nonlinearity in a computational model would be preferable for an accurate simulation of the vocal fold dynamics.

Acknowledgement

This research is sponsored by the NIDCD (Grant No. 5R01DC011338) and the NSF (Grant No. CBET-1066962).

References

- ¹ K. Ishizaka and J. L. Flanagan. Synthesis of voiced sounds from a two-mass model of the vocal cords. *Bell System Tech. J.*, 51:1233–1268, 1972.
- ² J.J. Jiang and Y. Zhang. Chaotic vibration induced by turbulent noise in a two-mass model of vocal folds. *J. Acoust. Soc. Am.*, 112(5):2127–2133, 2002.
- ³ Fariborz Alipour, Christoph Brucker, Douglas D Cook, Andreas Gommel, Manfred Kaltenbacher, Willy Mattheus, Luc Mongeau, Eric Nauman, Rudiger Schwarze, Isao Tokuda, et al. Mathematical models and numerical schemes for the simulation of human phonation. *Current Bioinformatics*, 6(3):323–343, 2011.
- ⁴ F. Alipour, D.A. Berry, and I.R. Titze. A finite-element model of vocal-fold vibration. *J. Acoust. Soc. Am.*, 14:442–454, 2000.
- ⁵ H. Luo, R. Mittal, and S. A. Bielamowicz. Analysis of flow-structure interaction in the larynx during phonation using an immersed-boundary method. *J. Acoust. Soc. Am.*, 126:816–824, 2009.
- ⁶ X. Zheng, Q. Xue, R. Mittal, and S. Bielamowicz. A coupled sharp-interface immersed-boundary-finite-element method for flow-structure interaction with application to human phonation. *Journal of biomechanical engineering*, 132(11):111003, 2010.
- ⁷ I.R. Titze. *Principles of voice production*. Prentice-Hall, Englewood Cliffs, NJ, 1994. 354 pages.
- ⁸ Brian A Pickup and Scott L Thomson. Identification of geometric parameters influencing the flow-induced vibration of a two-layer self-oscillating computational vocal fold model. *J. Acoust. Soc. Am.*, 129:2121, 2011.
- ⁹ Simeon L Smith and Scott L Thomson. Effect of inferior surface angle on the self-oscillation of a computational vocal fold model. *The Journal of the Acoustical Society of America*, 131:4062, 2012.
- ¹⁰ K. Zhang, T. Siegmund, and R.W. Chan. A constitutive model of the human vocal fold cover for fundamental frequency regulation. *J. Acoust. Soc. Am.*, 119:1050–1062, 2006.
- ¹¹ R.W. Chan, T. Siegmund, and K. Zhang. Biomechanics of fundamental frequency regulation: Constitutive modeling of the vocal fold lamina propria. *Logopedics Phoniatrics Vocology*, 34(4):181–189, 2009.
- ¹² J. F. Doyle. *Nonlinear analysis of thin-walled structures: statics, dynamics, and stability*. Springer-Verlag, New York, 2001. 511 pages.
- ¹³ H. Gunter. A mechanical model of vocal-fold collision with high spatial and temporal resolution. *J. Acoust. Soc. Am.*, 113:994–1000, 2003.
- ¹⁴ C. Tao, J.J. Jiang, and Y. Zhang. Simulation of vocal fold impact pressures with a self-oscillating finite-element model. *J. Acoust. Soc. Am.*, 119:3987–3994, 2006.

- ¹⁵ W. Goldsmith. *Impact: the theory and physical behavior of colliding solids*. 2001. 379 pages.
- ¹⁶ H. Luo, R. Mittal, X. Zheng, S. Bielamowicz, R. Walsh, and J. Hahn. An immersed-boundary method for flow–structure interaction in biological systems with application to phonation. *J. Comput. Phys.*, 227:9303–9332, 2008.
- ¹⁷ W.R. Zemlin. *Speech and hearing science: anatomy & physiology*. Allyn and Bacon, Boston, MA, 4th edition, 1997. 610 pages.
- ¹⁸ G.Z. Decker and S.L. Thomson. Computational simulations of vocal fold vibration: Bernoulli versus Navier-Stokes. *Journal of Voice*, 21(3):273, 2007.
- ¹⁹ I. R. Titze. Mechanical stress in phonation. *J. Voice*, 8(2):99–105, 1994.

P_{sub} (kPa)	0.5	0.6	0.7	0.8
Model I: f (Hz)	201.2	201.4	203.8	220.9
Model II: f (Hz)	198.7	202.6	202.5	202.3

TABLE I. Dominant vibration frequency of the vocal folds as simulated using the two models.

List of Figures

FIG. 1	A 2D model for studying the role of geometric nonlinearity in the vocal fold dynamics.	5
FIG. 2	The lowest four eignmodes of the current vocal fold model. (a) The 1st mode at $f_1 = 86.9$ Hz, (b) the 2nd mode at $f_2 = 192.2$ Hz, (c) the 3rd mode at $f_3 = 217.5$ Hz, and (d) the 4th mode at $f_4 = 372.9$ Hz. The dashed line is for the rest shape, and the solid line is for deformed shape.	7
FIG. 3	The time history of the glottal gap width for model II with $P_{\text{sub}} = 0.6$ kPa. (a) Initial transition period; (b) the established vibration.	7
FIG. 4	The vibration pattern of the vocal folds simulated by model I (a,b,c) and model II (d,e,f). The subglottal pressure is (a,d) $P_{\text{sub}} = 0.6$ kPa, (b,e) $P_{\text{sub}} = 0.7$ kPa and (c,f) $P_{\text{sub}} = 0.8$ kPa. The solid line and dashed line represent the open and closed phases, respectively. The circle shown in (a) is the marker point that will be used in the PSD analysis.	9
FIG. 5	The PSD analysis of the oscillation of a point at the medial surface for $P_{\text{sub}} = 0.7$ and 0.8 kPa. The two dashed lines indicate the eigenfrequencies f_2 and f_3	9
FIG. 6	(a) The gap width during the open phase versus P_{sub} . (b) The waveform of the gap width at $P_{\text{sub}} = 0.6$ kPa. In both (a) and (b), the dashed line is for model I and the solid line for model II.	10
FIG. 7	The impact stress (a) and the total contact force (per unit length in span) (b) during vocal fold collision. The dashed line is for model I and the solid line for model II.	11
FIG. 8	(a) The time-averaged flow rate (per unit span); (b) the waveform of the flow rate at $P_{\text{sub}} = 0.8$ kPa. The dashed line is for model I and the solid line for model II.	11
FIG. 9	Instantaneous vorticity contours during vocal fold opening for (a) model I and (b) model II at $P_{\text{sub}} = 0.8$ kPa.	12
FIG. 10	(a) Illustration of the load tests of the current vocal fold model. The reference point marked by a circle is used to measure the displacement. (b,c) p/P_{sub} from the FSI simulation during vocal fold opening for (b) $P_{\text{sub}} = 0.6$ kPa and (c) $P_{\text{sub}} = 0.8$ kPa.	13
FIG. 11	Displacement of the reference point in the static load test, the dynamic load test, and the coupled FSI simulation. (a) The total displacement; (b) the y -displacement.	13